

High-speed atomic force microscope imaging: Adaptive multiloop modeJuan Ren^{*} and Qingze Zou[†]*Department of Mechanical and Aerospace Engineering, Rutgers, The State University of New Jersey, 98 Brett Road, Piscataway, New Jersey 08854, USA*

Bo Li and Zhiqun Lin

School of Materials Science and Engineering, Georgia Institute of Technology, 3100K, Molecular Science & Engineering Building, Atlanta, Georgia 30332, USA

(Received 2 April 2014; published 28 July 2014)

In this paper, an imaging mode (called the adaptive multiloop mode) of atomic force microscope (AFM) is proposed to substantially increase the speed of tapping mode (TM) imaging while preserving the advantages of TM imaging over contact mode (CM) imaging. Due to its superior image quality and less sample disturbances over CM imaging, particularly for soft materials such as polymers, TM imaging is currently the most widely used imaging technique. The speed of TM imaging, however, is substantially (over an order of magnitude) lower than that of CM imaging, becoming the major bottleneck of this technique. Increasing the speed of TM imaging is challenging as a stable probe tapping on the sample surface must be maintained to preserve the image quality, whereas the probe tapping is rather sensitive to the sample topography variation. As a result, the increase of imaging speed can quickly lead to loss of the probe-sample contact and/or annihilation of the probe tapping, resulting in image distortion and/or sample deformation. The proposed adaptive multiloop mode (AMLM) imaging overcomes these limitations of TM imaging through the following three efforts integrated together: First, it is proposed to account for the variation of the TM deflection when quantifying the sample topography; second, an inner-outer feedback control loop to regulate the TM deflection is added on top of the tapping-feedback control loop to improve the sample topography tracking; and, third, an online iterative feedforward controller is augmented to the whole control system to further enhance the topography tracking, where the next-line sample topography is predicted and utilized to reduce the tracking error. The added feedback regulation of the TM deflection ensures the probe-sample interaction force remains near the minimum for maintaining a stable probe-sample interaction. The proposed AMLM imaging is tested and demonstrated by imaging a poly(*tert*-butyl acrylate) sample in experiments. The experimental results demonstrate that the image quality achieved by using the proposed AMLM imaging at a scan rate of 25 Hz and over a large-size imaging ($50\ \mu\text{m} \times 25\ \mu\text{m}$) is at the same level of that obtained using TM imaging at 1 Hz, while the probe-sample interaction force is noticeably reduced from that achieved using TM imaging at 2.5 Hz.

DOI: [10.1103/PhysRevE.90.012405](https://doi.org/10.1103/PhysRevE.90.012405)

PACS number(s): 68.37.-d, 07.79.Lh

I. INTRODUCTION

In this paper, an imaging mode (called the *adaptive multiloop mode*) of atomic force microscope (AFM) is proposed to substantially increase the speed of tapping mode (TM) imaging while preserving its advantages over contact mode (CM) imaging. TM imaging is the most widely used imaging technique of AFM, owing to its superior image quality and subdued sample distortion when compared to CM imaging [1–4]. The rather slow imaging speed, however, has become the major limitation and bottleneck of TM imaging [5,6]. High-speed TM imaging is challenging as an increase in imaging speed can quickly lead to a loss of the probe-sample interaction and/or annihilation of the cantilever tapping vibration, particularly when the imaging size is large. Current efforts to increase the speed of TM imaging [2,7], however, have only lead to rather limited improvements as the speed increase is rather small (around three times), and accompanied with a substantial (over

five times) increase of force applied. Thus, the challenges in and the needs for high-speed TM imaging motivate the development of the proposed imaging technique.

As been widely acknowledged, it is challenging to increase the speed of TM imaging. Central to TM imaging is to maintain the rms-tapping amplitude closely around the set point during the imaging [5,7]. Such a requirement, although it can be achieved when imaging at low speed (usually < 1 Hz), becomes challenging for rms-tapping-amplitude feedback control when the speed increases, as the time delay that is inevitably induced into the rms-tapping-amplitude feedback loop limits the response speed of the tapping-amplitude feedback loop to the sample topography variation [2,7]. Since the tapping amplitude is sensitive to the probe-sample distance variation, and the force-distance region of the TM imaging is highly nonlinear [8,9], the probe-sample distance variation can quickly lead to loss of probe-sample contact and annihilation of probe tapping when the imaging speed increases. Thus, the control scheme of TM imaging inherently limits its speed.

Current efforts to improve the imaging speed of TM imaging only results in rather limited improvements. For example, it has been proposed to utilize high bandwidth

^{*}juanren@rci.rutgers.edu[†]Author to whom correspondence should be addressed: qzzou@rci.rutgers.edu

piezo actuators and cantilevers with high resonant frequencies [10,11] to increase the TM-imaging speed up to ~ 2 mm/s [12]. The lateral size and the sample height that can be imaged, however, are both substantially reduced (from around $100 \mu\text{m} \times 100 \mu\text{m}$ to $30 \mu\text{m} \times 30 \mu\text{m}$, and from 10 to $3 \mu\text{m}$, respectively). Alternative to such a hardware-based approach that is accompanied with instrument cost increases, control techniques [7,13] such as the observer-based approach [14] have been developed to increase TM-imaging speed with minor or no additional cost. The speed increase achieved, however, is rather limited (e.g., < 1.8 mm/s [13,14]), or the speed is increased at the cost of image quality, and more seriously, without adequate control in the interaction force as in the observer-based approach [14]. Therefore, it still remains as a challenge to achieve high-speed, large-size imaging of the tapping mode with a well-controlled interaction force.

The proposed approach aims to not only substantially increase the TM-imaging speed without loss of image quality, but also maintain the probe tapping closely around the set point and the tip-sample interaction force around the minimal (needed for maintaining a stable tapping) throughout the imaging process. Such an improvement in both the imaging speed and the interaction force control is achieved through the development of an adaptive multiloop mode (AMLM) imaging scheme that regulates both the tapping amplitude and the mean cantilever deflection (called the *TM deflection* later). Specifically, the proposed AMLM imaging is composed of the following three ingredients: (i) Unlike conventional TM imaging that completely ignores the TM-deflection variation, it is proposed to take the variation of the cantilever TM deflection into account when quantifying the sample topography. (ii) Unlike TM imaging that only regulates the tapping amplitude via rms-amplitude feedback control, the proposed AMLM imaging explores an inner-outer feedback control loop to regulate the TM deflection on top of the rms-amplitude feedback. (iii) A data-driven online iterative feedforward controller is augmented to overcome the time delay of the rms-amplitude feedback loop, where the next-line sample topography and tracking error are predicted and utilized to further improve the topography tracking.

The experimental implementation of the proposed approach demonstrates that, compared to TM imaging, the proposed AMLM imaging not only increases the imaging speed by over tenfold, but at the same time also reduces the tip-sample interaction force by 35%. Using the proposed AMLM imaging, the average lateral scanning speed reaches 2.5 mm/s when imaging a poly(tert-butyl acrylate) (PtBA) sample (scan rate, 25 Hz; scan size, $50 \mu\text{m}$). Even at such a high speed, the image quality is maintained as that when using TM imaging at over 20-fold slower (1 Hz), with the tip-sample interaction force maintained around the minimal level.

The remainder of this paper is organized as follows. In Sec. II, our sample topography quantification is proposed and employed to reveal the drawbacks of AMLM imaging, followed by the proposed AMLM technique in Sec. III. The experimental implementation of the proposed AMLM imaging is described and discussed in comparison to conventional TM imaging in Sec. IV. The conclusions are given in Sec. V.

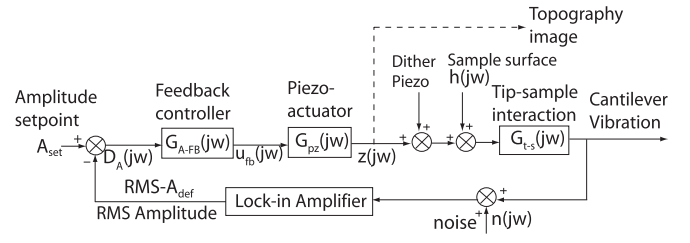


FIG. 1. Schematic block diagram of the rms-z-feedback control in conventional TM imaging.

II. ISSUES OF CONVENTIONAL TAPPING MODE IMAGING

TM imaging was developed to address the issues of contact mode imaging (CM imaging) caused by probe sliding [5,9] in imaging resolution and sample distortion [1,2], particularly for soft samples. Unlike in CM imaging, during TM imaging the cantilever probe is excited (usually using a small piezo stack actuator, called a dither piezo—see Fig. 1) to vibrate around its resonance and intermittently interact with the sample, i.e., tap on the sample surface. Then the rms amplitude of the cantilever vibration ($\text{rms-}A_{\text{def}}$) is measured using a lock-in amplifier, and maintained around the set-point value A_{set} through a feedback control system (see Fig. 1) using a piezoelectric actuator (called the *z*-piezo below). Provided that the sample topography profile is closely tracked by the cantilever probe during the scanning, signaling by the rms amplitude being close enough to the set-point value, the sample surface topography can be quantified as the *z*-piezo displacement. As virtually no probe sliding on the sample surface occurs during TM imaging, the sliding-related sample damage is largely avoided, and a higher imaging resolution can be achieved [5,15].

A. Limits of the rms-tapping-feedback control system

The speed of TM imaging, however, is inherently hindered by the limits of the *z*-axis feedback control system (called the *rms-z-feedback* below). As multiple periods of tapping are needed to measure the rms-tapping amplitude, time delay is inevitably induced in the rms-z-feedback loop, i.e., the measured rms-tapping amplitude differs from and lags behind the instantaneous tapping amplitude $A_{\text{def}}(t)$, especially when the tapping amplitude varies with the sample topography variation. Such a time delay, although it is relatively small and can be compensated for by the rms-z-feedback control when imaging at slow speeds, becomes more pronounced as the scan speed increases, and adversely affects the rms-z-feedback control in the sample profile tracking, leading to a large variation in the probe-sample distance.

The cantilever tapping, however, is sensitive to the change in the probe-sample distance [7,9], as in TM imaging the probe-sample interaction force is highly nonlinear with regard to the probe-sample distance (see Fig. 2). The probe-sample distance change due to the imaging speed increase can result in a loss of sample-probe contact and/or annihilation of tapping. Specifically, loss of probe-sample contact tends to occur around the sample regions where, e.g., sudden topography drops appear, and the cantilever tapping approaches free

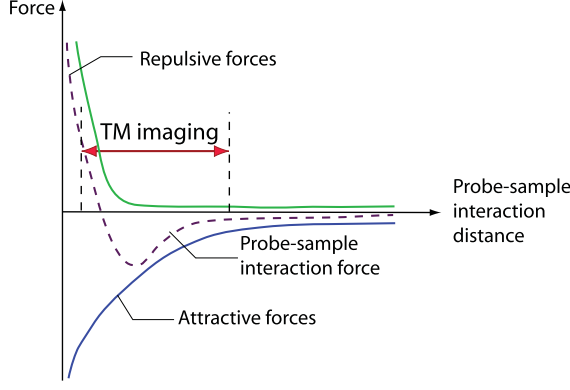


FIG. 2. (Color online) A schematic plot of probe-sample interaction distance vs the probe sample interaction force.

oscillation gradually with a relatively long settling time (due to the high- Q factor of the cantilever) [5,6]. Contrarily, tapping can be completely annihilated around the sample regions where, e.g., sharp topography increases exist, resulting in the probe sliding on the sample surface. Due to the time delay, it is, however, challenging to avoid the loss of probe-sample contact and annihilation of tapping during high-speed imaging. The time delay limits the use of a high feedback gain in the rms- z -feedback, as a high feedback gain tends to result in overshoot in the response [16,17], which, in turn, leads to the cantilever motion bouncing back and forth between the loss of contact and the annihilation of tapping. A small feedback gain, however, is also incapable of accounting for the loss of contact and/or annihilation of tapping as the imaging speed increases. Therefore, the control mechanism employed in TM imaging is not adequate for high-speed TM imaging.

Current efforts to improve the speed of TM imaging have resulted in rather limited progress. We note that the speed of TM imaging can be increased by choosing a larger free vibration amplitude and a smaller tapping-amplitude set point [2,7]. Such a choice, however, results in a much larger probe-sample interaction force. Given a cantilever probe with mass m , quality factor Q , and spring constant k_c , the probe-sample interaction force $F_{t-s}(t)$ during TM imaging can be estimated as [8,9]

$$F_{t-s}(t) = m\ddot{d}_{\text{tot}}(t) + \frac{m\omega_0}{Q}\dot{d}_{\text{tot}}(t) + k_c d_{\text{tot}}(t), \quad (1)$$

with

$$d_{\text{tot}}(t) = d_{\text{TM}}(t) + [A_{\text{def}} \cos(\omega_0 t + \phi) - A_{\text{free}} \cos(\omega_0 t)],$$

where $d_{\text{tot}}(t)$, $d_{\text{TM}}(t)$, and A_{free} are the total deflection, the mean deflection per vibration period (called *TM deflection*), and the free vibration amplitude of the cantilever, respectively. ϕ denotes the phase shift of the cantilever's response to the excitation. Thus, Eq. (1) clearly implies that the combination of a larger A_{free} and a smaller A_{def} increases the total probe-sample interaction force $F_{t-s}(t)$. Furthermore, this combination also implies a smaller probe-sample separation distance, resulting in a larger TM deflection, thereby, a larger average probe-sample interaction force per vibration period,

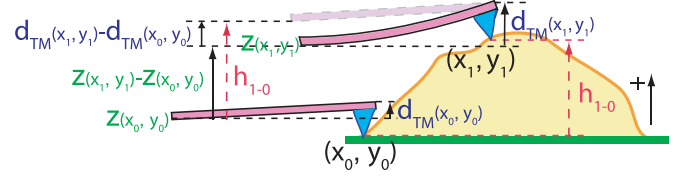


FIG. 3. (Color online) Height difference between two points on the sample surface during TM imaging.

i.e., [8,9]

$$\langle F_{t-s} \rangle = (1/T) \oint F_{t-s}(t) dt = k_c d_{\text{TM}}, \quad \text{with } T = 2\pi/\omega_0. \quad (2)$$

To overcome this constraint, it has been proposed to employ a high bandwidth z -piezo with active Q control to increase the TM-imaging speed [6,7]. The speed increase achieved, however, is rather limited ($\leq 300 \mu\text{m/s}$ at a scan size of $50 \mu\text{m}$) as the time delay of the rms-amplitude feedback is still the bottleneck—even though the loss of contact and the annihilation of tapping can be largely avoided, $d_{\text{TM}}(t)$ still varies substantially as the imaging speed increases, directly resulting in a large image distortion.

B. Topography quantification in TM imaging

We propose to quantify the sample topography by taking the TM deflection into account. Consider, during TM imaging, the probe-sample interaction at two different locations on the sample surface, point (x_0, y_0) and point (x_1, y_1) (see Fig. 3), and the z -piezo positions and the TM deflections at these two points are denoted as $z(x_0, y_0)$ and $z(x_1, y_1)$, and $d_{\text{TM}}(x_0, y_0)$ and $d_{\text{TM}}(x_1, y_1)$, respectively, then the height difference between these two points is given as

$$h_{1-0} = [z(x_1, y_1) - z(x_0, y_0)] + \varepsilon [d_{\text{TM}}(x_1, y_1) - d_{\text{TM}}(x_0, y_0)], \quad (3)$$

where ε is the contact constant that depends on the probe-sample interaction regime: $\varepsilon = -1$, when the probe-sample interaction is dominated by the long-range attractive force [e.g., $A_{\text{def}}/A_{\text{free}} \in (0.5, 0.8)$], $\varepsilon = 1$ when the repulsive probe-sample interaction force appears, and $-1 \ll \varepsilon < 0$ when the tapping amplitude is close to the free vibration amplitude, i.e., $A_{\text{def}} \approx A_{\text{free}}$. Thus, Eq. (3) implies that the sample topography of the entire imaged area can be obtained with respect to one fixed reference point, e.g., the first sample point imaged—for convenience. Without loss of generality, the height and deflection datum point can be set as $z(x_0, y_0) = 0$ and $d_{\text{TM}}(x_0, y_0) = d_{\text{TM-d}}$ (i.e., the TM deflection corresponding to the tapping amplitude at the set-point value), respectively, and the sample surface topography can be quantified as

$$\begin{aligned} h(x, y) &= z(x, y) + \varepsilon [d_{\text{TM}}(x, y) - d_{\text{TM-d}}] \\ &= z(x, y) + \varepsilon \Delta d_{\text{TM}}(x, y). \end{aligned} \quad (4)$$

Equation (4) clearly reveals the imaging errors in high-speed TM imaging. At slow imaging speeds, the cantilever probe can accurately follow the sample topography under the rms- z -feedback control, i.e., A_{def} is closely around the set-point value and the TM-deflection variation $\Delta d_{\text{TM}}(t)$ is small enough,

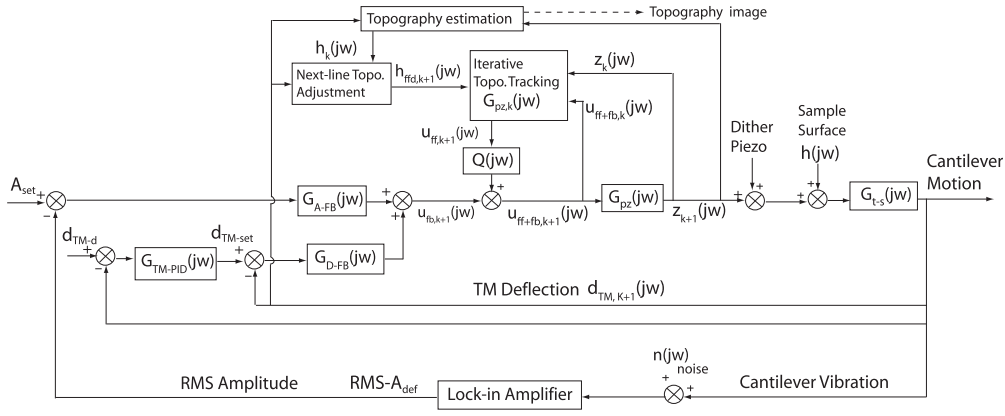


FIG. 4. Schematic block diagram of the proposed AMLM imaging.

hence, the sample topography can be adequately quantified as the z -piezo displacement, i.e., as $d_{TM}(x, y) \approx d_{TM-d}$, $h(x, y) \approx z(x, y)$ in Eq. (4). However, with an imaging speed increase it is challenging to maintain such a stringent condition ($A_{def} \approx A_{set}$). Even when the scanning speed increases slightly and no loss of contact or annihilation of tapping occurs, i.e., when the variation of the rms-tapping amplitude is small (the variation of the instantaneous tapping amplitude A_{def} , however, may not be negligible), variations of the TM deflection can still be pronounced, especially in so-called *soft tapping mode* imaging [2,18] (where the tapping amplitude of the cantilever is less than 50% of the free vibration amplitude), i.e., $d_{TM}(x, y) \neq d_{TM-d}$. The variation in TM deflection, not accounted for in conventional TM imaging, thereby directly leads to image distortion. Therefore, the conventional sample topography quantification also limits TM imaging.

We note that, although Eq. (4) implies the speed of TM imaging might be increased by accounting for the TM deflection in the sample topography quantification, such a modification does nothing to improve the sample topography tracking, i.e., as the imaging speed increases, the probe-sample interaction force $\langle F_{I-s} \rangle$ can vary dramatically and quickly leads to loss of contact and/or annihilation of tapping. Thus, maintaining the sample topography tracking is essential to high-speed TM imaging.

III. ADAPTIVE MULTILoop MODE IMAGING

We propose adaptive multiloop mode imaging (AMLM imaging) to address the above issues. In essence, in the proposed imaging mode, control of the z -axis motion of the probe combines the rms- z -feedback loop in TM imaging with the deflection feedback loop in CM imaging while maintaining the tapping amplitude of the probe as in TM imaging—the adaptive multiloop mode.

As depicted in Fig. 4, the proposed AMLM imaging introduces two major components on top of the rms- z -feedback loop to control the z -axis motion of the probe: (i) a feedback control in the inner-outer loop structure to regulate the TM deflection, and (ii) an online iterative feedforward controller to overcome the time delay of the rms- z -feedback loop in tracking the sample topography.

A. TM-deflection regulation: An inner-outer feedback control approach

The TM-deflection inner-outer feedback loop closely regulates the averaged (vertical) position of the cantilever in each tapping period around the desired value for maintaining stable tapping. Specifically, the outer loop regulates the TM-deflection set point $d_{TM-set}(\cdot)$ while the inner loop tracks the regulated TM-deflection set point. The outer loop employs the following proportional-integral-derivative (PID) type of control,

$$d_{TM-set}(j+1) = k_I d_{TM-set}(j) + k_P e_{TM}(j) + k_D [e_{TM}(j-1) - e_{TM}(j)], \quad (5)$$

with

$$e_{TM}(j) = d_{TM-d} - d_{TM}(j), \quad \text{and} \quad j = 2, \dots, N-1,$$

where N is the total number of sampling periods per image, and k_P , k_I , and k_D are the proportional, integral, and derivative coefficients, respectively. The desired TM deflection d_{TM-d} is determined by the ratio of the chosen tapping-amplitude set point to the free amplitude, A_{set}/A_{free} . To choose A_{set} and d_{TM} , the d_{TM} vs (A_{def}/A_{free}) relation is needed and can be measured *a priori*. A previous study [9] showed that the d_{TM} vs (A_{def}/A_{free}) relation resembles a parabolic curve centering around A_{def}/A_{free} at $\sim 50\%$. As can be seen from the exemplary d_{TM} vs (A_{def}/A_{free}) plot measured in this work shown in Fig. 5, the tip-sample interaction force increases significantly when the tapping ratio $A_{def}/A_{free} < 10\%$, whereas when A_{def}/A_{free}

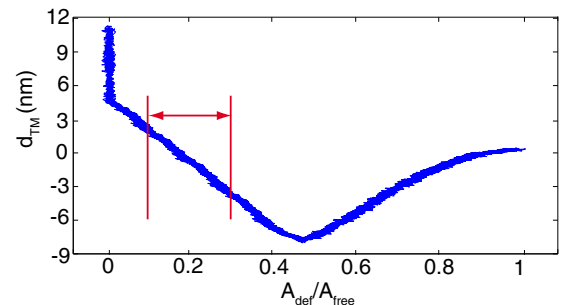


FIG. 5. (Color online) d_{TM} vs A_{def}/A_{free} .

is larger than 80%, the increase of the scanning speed can quickly lead to the loss of contact. Thus, for the d_{TM} vs (A_{def}/A_{free}) plot shown in Fig. 5, the A_{set} shall be chosen around 10%–30% A_{free} (since the corresponding tip-sample interaction force is small), and the desired TM deflection is then picked according to Fig. 5.

B. Online iterative feedforward control for sample-topography tracking

To further enhance the tracking of the sample topography, and thereby the imaging speed, an online iterative feedforward controller of the piezo actuator is integrated to the rms- z -feedback loop (see Fig. 4) by implementing the following the high-order modeling-free difference-inversion-based iterative-control (HOMDIIC) algorithm [19] online,

$$\begin{aligned} U_{ff,0}(j\omega) &= 0, \\ U_{ff,1}(j\omega) &= \frac{U_{ff+fb,0}(j\omega)}{Z_0(j\omega)} H_{ffd,1}(j\omega), \\ U_{ff,k+1}(j\omega) &= U_{ff,k} + \lambda \frac{U_{ff+fb,k}(j\omega) - U_{ff+fb,k-1}(j\omega)}{Z_k(j\omega) - Z_{k-1}(j\omega)} e_k(j\omega), \\ k &\geq 1, \\ e_k(j\omega) &= H_{ffd,k+1}(j\omega) - Z_k(j\omega), \end{aligned} \quad (6)$$

where $j\omega$ denotes the Fourier transform of the corresponding signal, λ is a prechosen constant to ensure the convergence of the iteration, and $U_{ff+fb,k}(\cdot)$ and $Z_k(\cdot)$ are the total control input (feedback+feedforward) applied to the z -piezo actuator [i.e., $U_{ff+fb,k}(j\omega) = U_{ff,k}(j\omega) + U_{fb,k}(j\omega)$ —see Fig. 4] and the z -piezo displacement measured on the k th scan line, respectively, and $H_{ffd,k+1}(\cdot)$ denotes the desired trajectory that the z -piezo needs to track at the $(k+1)$ th scan line. Note that the ratios in the above control law, $U_{ff+fb,0}(j\omega)/Z_0(j\omega)$ and $[U_{ff+fb,k}(j\omega) - U_{ff+fb,k-1}(j\omega)]/[Z_k(j\omega) - Z_{k-1}(j\omega)]$, essentially equal the inverse of the frequency response of the z -piezo actuator, and are updated line by line iteratively throughout the imaging process. Such a data-driven online-updated inverse is preferred over an *a priori*-obtained fixed model in the iterative scheme [20,21] for better robustness and tracking performance [22]. The feedforward input for the next scan line, $U_{ff,k+1}(j)$ for $j = 1, \dots, N_l$ (N_l is the total number of sampling points per scan line), was computed during the sampling period between the last sampling point of the current scan

line and the first sampling point of the next scan line by using the HOMDIIC algorithm [Eq. (6)] in the frequency domain directly via the discrete Fourier transform and discrete inverse Fourier transform. The computed $U_{ff,k+1}(\cdot)$ was then applied one point at a (sampling) time during the next-line imaging.

The other feature of the above feedforward controller is that the desired trajectory to track in Eq. (6), $H_{ffd,k}(\cdot)$, accounts for both the predicted sample topography and the predicted next-line TM-deflection tracking error. Specifically, at the end of the k th line scanning, the sample topography profile of the $(k+1)$ th scan line $h_{k+1}(t)$ is approximated as that of the k th scan line [quantified via Eq. (4)], i.e., $h_{k+1}(t) \approx h_k(t)$. Such an approximation is reasonable as with enough scan lines, the line-to-line topography variations are small. Similarly, the TM-deflection tracking error on the $(k+1)$ th scan line is predicted (approximated) as that on the k th, $d_{TM,k}(\cdot) - d_{TM-d}$, if the same control were applied. Then, the next-line desired trajectory $h_{ffd,k+1}(t)$ is obtained by combining the above two predictions as follows,

$$h_{ffd,k+1}(j) = h_k(j) + \alpha[d_{TM,k}(j) - d_{TM-d}], \quad j = 1, \dots, N_l, \quad (7)$$

where N_l and α are the total sampling points per scan line and the correction factor, respectively.

The TM deflection is introduced in the above iterative algorithm [Eq. (7)] to reduce the amplitude of the interaction force when the imaging sample areas of rapid and large topography change (vertically). Note that the TM deflection responds faster to the sample topography changes than the tapping amplitude. However, due to the compliance of the cantilever and the cantilever fixture (connecting the cantilever to the piezo actuator), a time delay still exists between the cantilever deflection change and that of the topography profile. As the scanning speed increases, such a time delay, albeit small, becomes crucial, and as a result, the spikes in the TM deflection reach their (local) peaks *after* the probe already passes these sample locations. Even with advanced feedback control, such deflection spikes still exist [23,24]. The above modified desired trajectory—for the feedforward control input to track—enables the z -piezo to drive the cantilever to respond in advance (i.e., preactuate) to the topography change, thereby reducing the amplitude of the deflection spikes. The correction

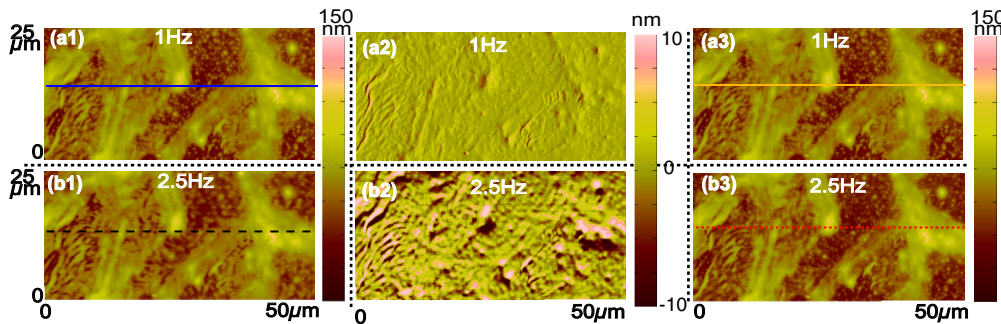


FIG. 6. (Color online) Sample topography images (scan area, $50 \mu\text{m} \times 25 \mu\text{m}$; scan direction, $50 \mu\text{m}$) obtained by using the TM imaging at the scan rate of (a1) 1 Hz and (b1) 2.5 Hz; the corresponding TM deflection measured at (a2) 1 Hz and (b2) 2.5 Hz; and the corresponding sample topography quantified using Eq. (4) at (a3) 1 Hz and (b3) 2.5 Hz.

factor α can be tuned based on the estimated height of the sample surface features.

During the imaging process, the above iterative scheme is applied repetitively to scan on the first line until the convergence is reached, i.e., until the difference in the z -piezo displacement between two consecutive iterations is small enough, e.g., close to the noise level (our experiments below show that only a couple of repetitive scans on the first line were needed). Then the converged input is used as the initial input for the iteration on the next scan line. Provided that the correction rate of the iterative input (i.e., the convergence rate) is faster than line to line, the input change caused by the sample topography change, the iterative control input only needs to be updated once, i.e., the rest of the sample can be imaged without iteration. A similar idea has been explored recently [24,25]. However, unlike the work in Refs. [24,25] that used a *fixed* model of the closed-loop dynamics, we propose here to use and update (using the measured input-output data) the frequency response of the z -axis piezo actuator itself. The use of the z -piezo dynamics itself provides a larger “working” bandwidth, i.e., a better tracking performance at high speed, as the feedback controller tends to reduce the open-loop bandwidth. Our experimental implementation below (see Sec. IV) demonstrates such an improvement.

Finally, to avoid noise being fed back into the closed loops via the feedforward channel, the feedforward control input $U_{ff,k+1}(\cdot)$ is passed through a zero-phase low-pass filter $Q(j\omega)$,

$$\begin{aligned}\hat{U}_{ff,k+1}(j\omega) &= Q(j\omega)U_{ff,k+1}(j\omega) \\ &= Q_b(j\omega)C_{lead}(j\omega)U_{ff,k+1}(j\omega),\end{aligned}\quad (8)$$

where $Q_b(j\omega)$ and $C_{lead}(j\omega)$ are a low-pass filter and a phase-lead compensator, respectively. As the entire next-line feedforward control input is known *a priori*, the above noncausal zero-phase filter can be implemented online.

The added TM-deflection feedback loop along with the feedforward controller substantially accelerates the tracking of the sample topography during imaging. Maintaining the TM deflection around the desired value helps to maintain the rms-tapping amplitude around the set point, particularly around the set point at which the corresponding TM deflection is minimal, resulting in the averaged probe-sample interaction force $\langle F_{t-s} \rangle$ being minimized. In this experiment, $A_{def}/A_{free} = 20\%$ was chosen so that $d_{TM-d} \approx 0$ (see Fig. 5). Moreover, by tracking the optimal predicted sample topography profile with rapid

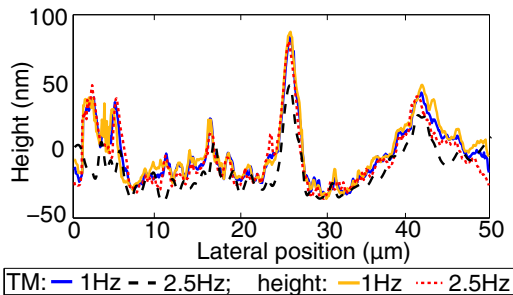


FIG. 7. (Color online) Comparison of the cross sections at the same scan line of the three images as marked out in Figs. 6(a1), 6(a3), and 6(b3).

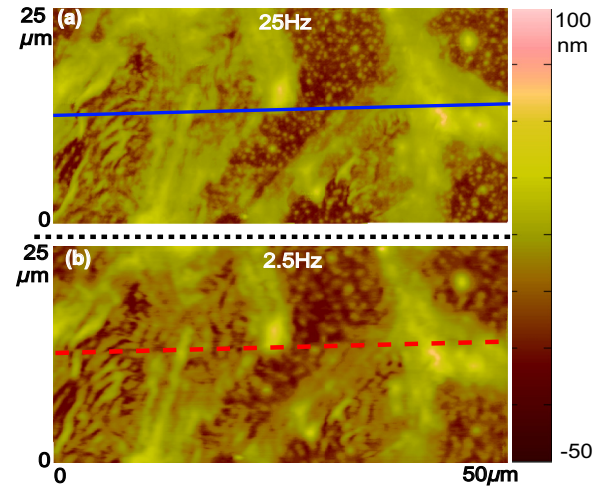


FIG. 8. (Color online) Top-view plot (i.e., image) of the z -piezo displacement obtained using (a) the proposed AMLM-imaging technique at a scan rate of 25 Hz and (b) TM imaging at a scan rate of 2.5 Hz, respectively.

convergence, the feedforward controller further reduces the tapping-amplitude oscillations upon sudden sample topography variation when the scanning speed increases. Therefore, the proposed TM-deflection loop along with data-driven iterative feedforward control play a major role in improving the quality and interaction force control of TM imaging.

IV. EXPERIMENTAL IMPLEMENTATION AND DISCUSSION

A sample of random and irregular patterns of poly(tert-butyl acrylate) (PtBA) on a silicon substrate was imaged at both small- and large-size imaging (20 and 50 μm , respectively) to validate and demonstrate the proposed technique, by comparing to TM imaging at a much lower speed. The sample was prepared by quickly evaporating a droplet of 20 μL PtBA solution at 1 mg/ml concentration on a hot silicon substrate. Under both the “coffee-ring” effect [26] and the fingering instability [27] during the evaporation, a sample

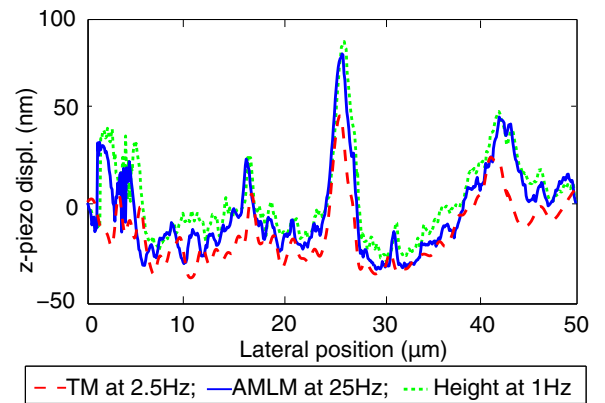


FIG. 9. (Color online) Comparison of the z -piezo displacement profile at the same cross-section location as marked out in Figs. 8(a), 8(b), and 6(a3).

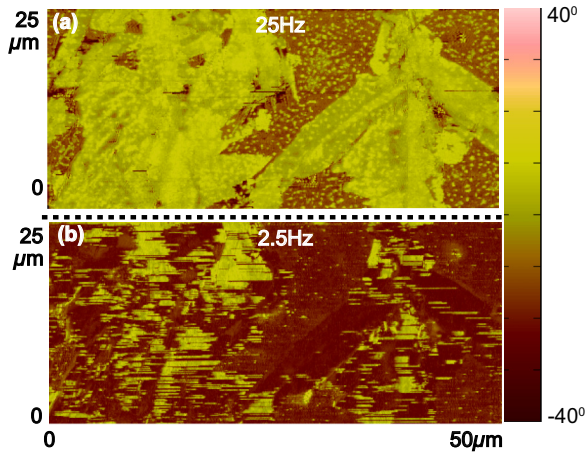


FIG. 10. (Color online) Phase images obtained using (a) the proposed AMLM-imaging technique at a scan rate of 25 Hz and (b) TM imaging at a scan rate of 2.5 Hz, respectively.

topography of large-scale (vertically and horizontally) PtBA aggregation and randomly distributed nanometer-size dots coexisting side by side was produced, well suited for evaluating and demonstrating the proposed AMLM-imaging technique.

A. Implementation of the AMLM-imaging technique

The experiments were conducted on a commercial AFM (Dimension Icon, Bruker AXS, Inc.) on which both the drive of the piezo actuators and all of the sensor signals including the TM deflection and the piezo displacement sensor signals can be directly accessed. All of the signals were acquired through a computer-based data acquisition system (NI-6259) under the Matlab xPC-target environment.

Throughout the imaging experiments, the HODMIIC technique was employed to achieve precise tracking in the lateral x - y axes scanning [19] by maintaining the tracking error below 1%. Moreover, the cross-axis dynamics coupling (mainly from the lateral x - y axes to the vertical z axis [28]) was compensated for by subtracting it from the z -piezo displacement measured. The PID controller parameters in Eq. (5) were set at $k_P = 1$, $k_I = 1$, and $k_D = \rho$, where ρ was a constant chosen *a priori*—the sample point-to-point gradient factor. Therefore, the

differences in topography tracking, the tip-sample interaction force, the tapping amplitude, and the image quality presented below reflect the effects of the proposed sample topography quantification and the proposed AMLM-imaging approach over the conventional TM imaging.

B. Sample topography quantification comparison

Experiments were conducted to validate the proposed topography quantification [Eq. (4)] first. As an example, results obtained at scan rates of 1 and 2.5 Hz over an imaging area of $50 \mu\text{m} \times 25 \mu\text{m}$ are compared for the z -piezo displacement images (i.e., the sample “topography” obtained in TM imaging) in Figs. 6(a1) and 6(b1), the TM deflection $d_{\text{TM}}(x, y)$ in Figs. 6(a2) and 6(b2), and the true sample topography images quantified by Eq. (4) in Figs. 6(a3) and 6(b3), respectively. Moreover, the cross-section z -piezo displacement and the sample topography profile quantified by using Eq. (4) at a randomly selected location are also compared in Fig. 7 for these two scan rates.

At a low imaging speed of 1 Hz, the sample topography can be quantified by using TM imaging, i.e., the z -piezo displacement [see Fig. 6(a1)]. The averaged relative difference between the TM image [Fig. 6(a1)] and the topography image [Fig. 6(a3)] by using Eq. (4) was only $\sim 4\%$ (see Fig. 7). As the imaging speed increases to 2.5 Hz, however, the sample topography cannot be accurately tracked by rms- z -axis feedback control alone. As a result, the average tip-sample interaction force was increased by over threefold compared to that obtained during the 1 Hz TM imaging [compare Fig. 6(a2) to Fig. 6(b2)]. With such a significant tip-sample interaction force increase, the TM image (the z -piezo displacement) at the scan rate of 2.5 Hz was 23% less accurate than the sample topography at the scan rate of 1 Hz quantified using Eq. (4). The image quality, however, was restored using the proposed topography quantification [Eq. (4)]. As shown in Fig. 6(b3), the difference between the low-speed and the high-speed scan was less than 7%. [Compare Fig. 6(b3) to Figs. 6(a3) and 6(b1), particularly those small dots distributed around the upper right region of the images. Also see the cross-section comparison in Fig. 7.] The probe-sample interaction force increased dramatically (over threefold) as the scan rate increased from 1 to 2.5 Hz [compare Fig. 6(a2) to Fig. 6(b2)]. Therefore, the

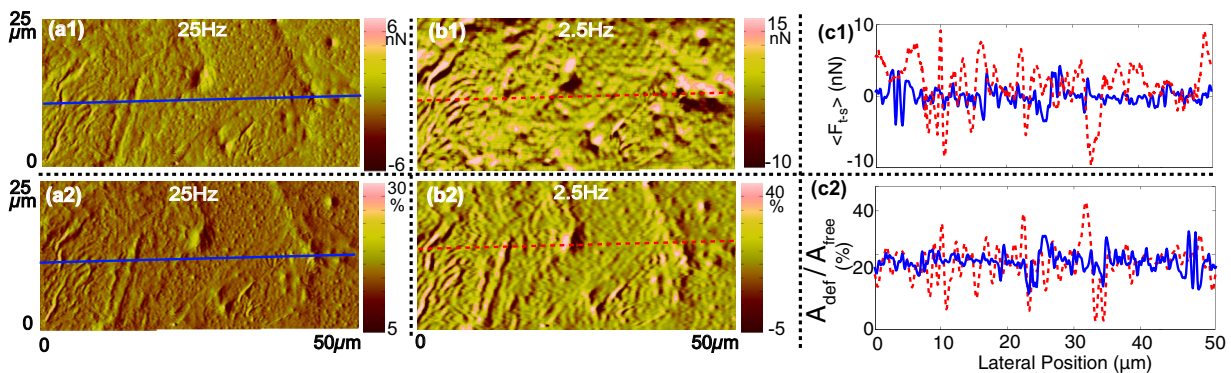


FIG. 11. (Color online) Comparison of the averaged probe-sample interaction force (i.e., the TM deflection) (a1) by using AMLM imaging at 25 Hz to (a2) that by using TM imaging at 2.5 Hz, and (b1), (b2) the images of the corresponding tapping-amplitude ratio ($A_{\text{def}}/A_{\text{free}}$), and the comparisons of (c1) the averaged force and (c2) the tapping-amplitude ratio at the cross section location marked in (a1) to (b2).

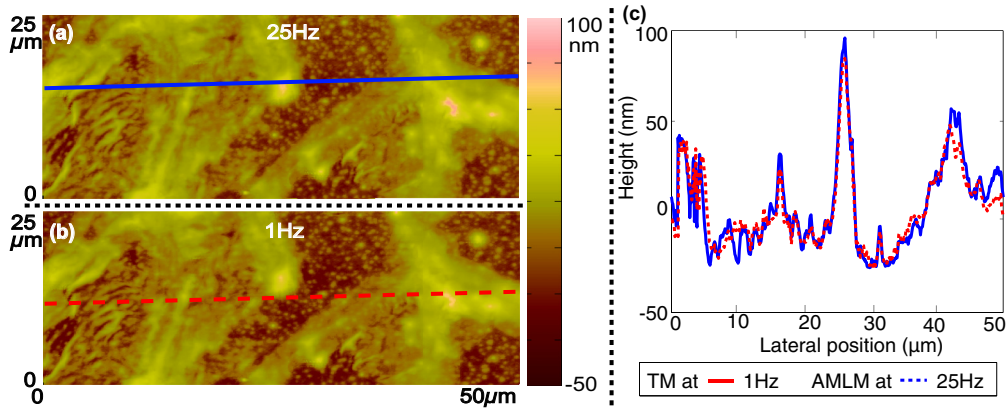


FIG. 12. (Color online) Comparison of the topography image obtained (a) using the proposed AMLM-imaging technique at the scan rate of 25 Hz to (b) the TM image at 1 Hz and (c) comparison of the corresponding topography profile cross sections.

experimental results demonstrated that the sample topography profile in TM imaging can be accurately quantified by using the proposed method [Eq. (4)], while the substantial force increase clearly manifested the limits of TM imaging.

C. High-speed near-minimum-force AMLM imaging

With the proposed sample topography quantification being validated, the proposed AMLM imaging was implemented to image the PtBA sample at a scan rate of 25 Hz (the average lateral scanning speed 2.5 mm/s), and then compared to the results obtained using TM imaging at 2.5 Hz. The z -piezo displacement images, the cross sections of the z -piezo displacement images, and the phase images obtained using these two methods are compared in Figs. 8–10, respectively. The z -piezo displacement comparison shows that the proposed AMLM imaging can track the sample topography more accurately at a scan rate of 25 Hz than TM imaging at a scan rate of 2.5 Hz. For example, those small dots near the upper right region of the image were sharper in Fig. 8(a1) than those in Fig. 8(a2). More specifically, by using AMLM imaging at 25 Hz, the relative difference between the z -piezo displacement in Fig. 8(a) and the sample height quantified in Fig. 6(a3) at a randomly selected cross section (marked by the dashed lines in Fig. 8) was three times smaller than that of using TM imaging at 2.5 Hz (<8% vs 24%—see Fig. 9). Furthermore, the comparison of the phase images in Figs. 10(a) and 10(b) also confirmed that the sample details through the phase contrast were largely distorted when using TM imaging at 2.5 Hz, whereas they were clearly preserved and presented when using AMLM imaging at 25 Hz. Therefore, the experimental results demonstrated that the proposed AMLM-imaging technique substantially improved the sample topography tracking. Such an improvement in sample topography tracking provided the opportunity to further reduce the tip-sample interaction force.

We further evaluated AMLM imaging in maintaining the near-minimum interaction force during imaging by regulating the TM-deflection set point and maintaining the tapping amplitude. The TM-deflection set point was updated at every sampling point according to Eq. (5). The images of the averaged force (i.e., the TM deflection) measured by using

AMLM imaging at 25 Hz and TM imaging at 2.5 Hz are compared in Figs. 11(a1) and 11(b1), respectively. The tapping-amplitude set point for both the imaging processes was chosen at 20% of the free vibration amplitude (with the corresponding TM deflection $d_{TM-d} \approx 0nN$ —see Fig. 5), and images of the tapping-amplitude ratio measured in these two cases are compared in Figs. 11(a2) and 11(b2), respectively. Also, the cross-section force and tapping-amplitude ratio variation at a randomly selected location are compared in Figs. 11(c1) and 11(c2), respectively.

The experimental results clearly demonstrate that both the averaged force and the tapping-amplitude fluctuation were substantially reduced by using the inner-outer feedback loop control of the TM deflection along with the online iterative feedforward control in the proposed AMLM imaging. The averaged force and the tapping-amplitude ratio mainly stayed in the regions of ± 5 nN and 15%–25%, respectively, when using AMLM imaging at 25 Hz, compared to the regions of -10 to 15 nN and 0%–40%, respectively, when using TM imaging at 2.5 Hz. More specifically, at the cross section (randomly selected) marked in Fig. 11, the amplitude of the averaged force and the fluctuation of the tapping amplitude of the 25 Hz AMLM imaging were 37% and 20% lower than those of the 2.5 Hz TM imaging [see Figs. 11(c1) and 11(c2), respectively]. Therefore, the proposed AMLM

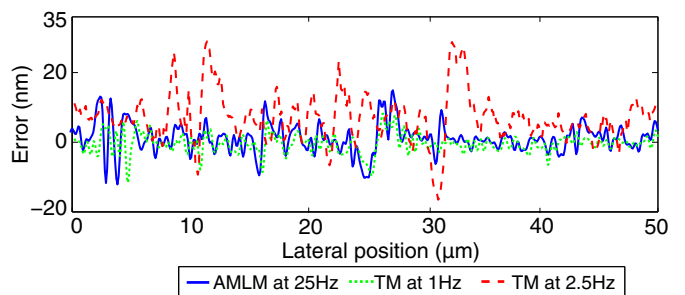


FIG. 13. (Color online) Comparison of the sample topography error obtained using the proposed AMLM imaging at 25 Hz to those obtained by using TM imaging at 1 and 2.5 Hz [with respect to the sample topography at the 1 Hz TM scan quantified via Eq. (4)].

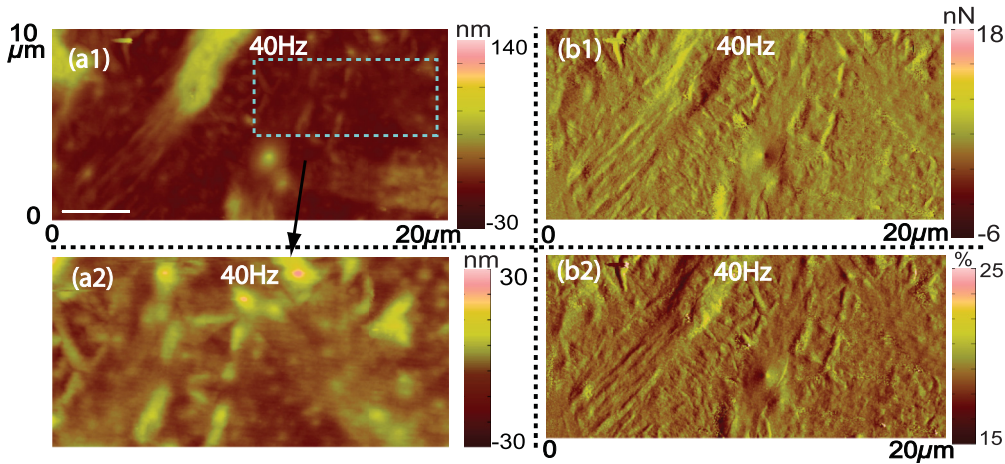


FIG. 14. (Color online) The sample topography image obtained using the proposed AMLM imaging at (a1) 40 Hz and (a2) the zoomed-in image, and images of the corresponding (b1) averaged force and (b2) the tapping-amplitude ratio ($A_{\text{def}}/A_{\text{free}}$), respectively.

imaging substantially reduced the probe-sample interaction force in TM imaging as well.

Finally, the image quality of the proposed AMLM-imaging technique was evaluated, as shown in Fig. 12, where the sample topography image obtained by using AMLM imaging at 25 Hz is compared to that obtained using TM imaging at 1 Hz. It can be seen that the image quality of the topography obtained by using the AMLM technique at 25 Hz was almost the same as that obtained by TM imaging at 1 Hz—both images presented almost the same details of the sample surface [compare Fig. 12(a) to Fig. 12(b)], whereas those details were degraded in the TM image at the scan rate of 2.5 Hz, as shown in Fig. 6(b1). The cross section of the topography image further confirmed these observations—the topography difference [with respect to the topography of the 1 Hz TM scan obtained by using Eq. (4)] obtained using AMLM imaging at 25 Hz was 20% smaller than that obtained using the TM at 2.5 Hz (see Fig. 13). We realize that such a substantial imaging speed increase—25-fold—with the image quality maintained was achieved at the cost of increased probe-sample interaction force. The force increase, however, was rather small—the rms total interaction force [quantified by Eq. (2)] during the imaging was only increased by 18%, and was 35% smaller than that of TM imaging at 2.5 Hz. Therefore, the experimental results demonstrated the efficacy of AMLM imaging in substantially increasing the imaging speed of TM imaging.

To further evaluate and demonstrate the proposed AMLM imaging, images of the sample over a smaller size ($20 \mu\text{m} \times 10 \mu\text{m}$) were also obtained using AMLM imaging at a scan rate of 40 Hz, as shown in Fig. 14, respectively. The topography images [Figs. 14(a1) and 14(a2)] showed that both the taller and lower sample surface features were captured consistently, and the averaged force and the tapping amplitude were maintained closely around the desired values. Particularly, the amplitude of the averaged force was maintained below 10 nN during most of the imaging process, substantially lower than the averaged force (23 nN) exerted in TM imaging at a much lower scan rate of 2.5 Hz [compare Fig. 14(b1) with Fig. 11(c1)], and the tapping-amplitude ratio was well

controlled around 20% throughout the whole image, as shown in Figs. 14(b2).

In summary, the experimental results demonstrated that the proposed AMLM-imaging technique increased the imaging speed by over tenfold while substantially lowering the tip-sample interaction force during the imaging closely around the minimal level needed to maintain a stable tapping of the probe.

V. CONCLUSION

Adaptive multiloop mode (AMLM) imaging is proposed to substantially improve the speed of tapping mode imaging. The proposed AMLM imaging combines the cantilever deflection control in CM imaging with the tapping-amplitude control in TM imaging while maintaining the tapping motion of the probe as in TM imaging. First, both the z -piezo displacement and the TM deflection are used to quantify the sample topography. Then, a feedback control loop of inner-outer loop structure is augmented to regulate the TM deflection around the minimal level for maintaining a stable probe tapping during the imaging, and a data-driven online iterative learning feedforward controller is integrated to the feedback loop to further improve the tracking of the sample topography. The efficacy of the proposed AMLM imaging was demonstrated by imaging a PtBA sample at different scanning speeds (25 and 40 Hz) and different imaging sizes (50 and $20 \mu\text{m}$). The comparisons of the sample topography tracking performances, the averaged tip-sample interaction forces, and the tapping-amplitude fluctuation between the proposed AMLM-imaging and the TM-imaging results showed that by using the proposed AMLM-imaging technique, the imaging speed was significantly increased by over tenfold over large-size imaging, and the tip-sample interaction force was substantially reduced.

ACKNOWLEDGMENT

The financial support of NSF CAREER Award Grant No. CMMI-1066055 is gratefully acknowledged.

- [1] A. Khurshudov, K. Kato, and H. Koide, *Wear* **203**, 22 (1997).
- [2] G. Bar, Y. Thomann, R. Brandsch, H. Cantow, and M. Whangbo, *Langmuir* **13**, 3807 (1997).
- [3] Y. Gan, *Surf. Sci. Rep.* **64**, 99 (2009).
- [4] R. García, R. Magerle, and R. Perez, *Nat. Mater.* **6**, 405 (2007).
- [5] H. Butt, B. Cappella, and M. Kappl, *Surf. Sci. Rep.* **59**, 1 (2005).
- [6] T. Sulchek, R. Hsieh, J. D. Adams, G. G. Yaralioglu, S. C. Minne, C. F. Quate, J. P. Cleveland, A. Atalar, and D. M. Adderton, *Appl. Phys. Lett.* **76**, 1473 (2000).
- [7] T. Sulchek, G. G. Yaralioglu, and C. F. Quate, *Rev. Sci. Instrum.* **73**, 2928 (2002).
- [8] Á. San Paulo and R. García, *Phys. Rev. B* **64**, 193411 (2001).
- [9] C. Su, L. Huang, and K. Kjoller, *Ultramicroscopy* **100**, 233 (2004).
- [10] B. Rogers, T. Sulchek, K. Murray, D. York, M. Jones, L. Manning, S. Malekos, B. Beneschott, J. Adams, H. Cavazos *et al.*, *Rev. Sci. Instrum.* **74**, 4683 (2003).
- [11] L. Picco, L. Bozec, A. Ulcinas, D. Engledew, M. Antognozzi, M. Horton, and M. Miles, *Nanotechnology* **18**, 044030 (2007).
- [12] Bruker Corporation, “Dimension fastscan”, 2011, <http://www.bruker.com/products/surface-analysis/atomic-force-microscopy/dimension-fastscan/learn-more.html>.
- [13] N. Kodera, M. Sakashita, and T. Ando, *Rev. Sci. Instrum.* **77**, 083704 (2006).
- [14] D. R. Sahoo, A. Sebastian, and M. V. Salapaka, *Appl. Phys. Lett.* **83**, 5521 (2003).
- [15] L. Wang, *Appl. Phys. Lett.* **73**, 3781 (1998).
- [16] J. Sloss, I. Sadek, J. Bruch, Jr., and S. Adali, *Dyn. . Stab. Syst.* **7**, 173 (1992).
- [17] S. Eckehard and H. G. Schuster (eds.), in *Handbook of Chaos Control* (John Wiley & Sons, New York, 2008).
- [18] R. Garcia and A. San Paulo, *Phys. Rev. B* **60**, 4961 (1999).
- [19] Z. Wang and Q. Zou, in *ASME Proceedings on Dynamic Systems and Control Conference, Palo Alto, California, USA, 2013* (ASME, New York, 2013), pp. V003T37A003–V003T37A003.
- [20] S. Tien, Q. Zou, and S. Devasia, *IEEE Trans. Control Syst. Technol.* **13**, 921 (2005).
- [21] Y. Wu and Q. Zou, *IEEE Trans. Control Syst. Technol.* **15**, 936 (2007).
- [22] K. Kim and Q. Zou, *IEEE Trans. Mechatronics* **18**, 1767 (2013).
- [23] Q. Zou, K. Leang, E. Sadoun, M. Reed, and S. Devasia, *Asian J. Control* **6**, 164 (2004).
- [24] Y. Wu and Q. Zou, *J. Dyn. Syst., Meas., Control* **131**, 061105 (2009).
- [25] Y. Wu, Q. Zou, and C. Su, *IEEE Trans. Nanotechnol.* **8**, 515 (2009).
- [26] R. D. Deegan, O. Bakajin, T. F. Dupont, G. Huber, S. R. Nagel, and T. A. Witten, *Nature (London)* **389**, 827 (1997).
- [27] A. Golovin, B. Rubinstein, and L. Pismen, *Langmuir* **17**, 3930 (2001).
- [28] Y. Yan, H. Wang, and Q. Zou, *Automatica* **48**, 167 (2012).